Journal of Nuclear Materials 458 (2015) 138–145

Contents lists available at ScienceDirect

Journal of Nuclear Materials

journal homepage: www.elsevier.com/locate/jnucmat

Primary radiation damage near grain boundary in bcc tungsten by molecular dynamics simulations

C.G. Zhang [a], W.H. Zhou [a], Y.G. Li [a,b], Z. Zeng [a,b,*], X. Ju [c]

[a] Key Laboratory for Materials Physics, Institute of Solid State Physics, Chinese Academy of Sciences, Hefei 230031, China
[b] Department of Physics, University of Science and Technology of China, Hefei 230026, China
[c] Department of Physics, University of Science and Technology Beijing, Beijing 100082, China

ARTICLE INFO

Article history:
Received 1 August 2014
Accepted 13 November 2014
Available online 17 December 2014

ABSTRACT

Molecular dynamics (MD) cascade simulations of single crystal and five bi-crystal structures in bcc tungsten (W) are conducted to investigate the role of grain boundaries (GBs) on defect production and the size distribution of defect clusters. The cascades in W with cascade energies of 10 keV and 20 keV are simulated at different distances from the GB plane at 4.2 K, 300 K and 900 K, respectively. The results indicate that the defect production is sensitive to the specific distance between the PKA and the nearby GB. The size of vacancy clusters becomes larger when the overlap region between the cascade and GB is small. Meanwhile, the mean size of interstitial clusters becomes smaller. The number of interstitials decreases with increasing temperature, whereas the number of vacancies is independent of the temperature.

1. Introduction

The irradiation of metals under MeV neutrons produces vacancies and interstitials [1,2] that can form clusters, such as cavities and dislocation loops, directly or indirectly [3–6]. These point defect evolution processes may lead to a series of macroscopic changes in the shape and properties of the materials, such as swelling, hardening or amorphization, which may severely affect the lifetime and reliability of the material for nuclear energy applications [7–10]. Interfaces in materials such as grain boundaries (GBs) can serve as sinks for absorbing and annihilating radiation-induced defects [11,12]. Many experiments have demonstrated that nano-structured metals have enhanced radiation tolerance compared to their bulk counterparts, such as nano-crystals [11,13–16] and nano-layers [17]. Computer modeling has been commonly used to investigate defect production and annealing near interfaces [12,18,19]. In particular, molecular dynamics (MD) simulations of collision cascades near GBs in metals have shown that interstitials are preferentially absorbed by GBs over vacancies during the picosecond (ps) timescale of the defect production stage [12,19]. During long-time defect annealing, temperature accelerated dynamics simulations have shown that some interstitials absorbed by GBs during defect production may be emitted and recombine with bulk vacancies [12]. Absorption of interstitials by GB and subsequent emissions to remove surviving vacancies are the fundamental micro-mechanisms of enhanced radiation tolerance for materials with large densities of GBs at relatively high temperatures [12,13].

Tungsten-based alloys are considered potential plasma-facing materials in tokamak fusion devices mainly because of their high melting temperature, high thermal conductivity and low sputtering erosion [20–23]. Many experiments have been done on the radiation effects on tungsten (W) [3,5,24,25]. Jäger and Wilkens observed the formation of vacancy-type dislocation loops in W produced by irradiation with 60 keV Au ions [3]. Yi et al. found the formation of vacancy loops within individual cascades through a collapse process by performing *in situ* self-ion irradiation experiments in W and W-5Re [5]. In terms of computational simulations, MD simulations were used to study the influence of the W empirical interatomic potential on the type and amount of radiation damage [26,27], which revealed that different types of potentials produce similar results of collision cascades even though their displacement thresholds are different. MD simulations were also performed to clarify the effect of temperature [26], showing that the amount of defects decreases with an increase in temperature. Sand et al. found a scale-less power-law-type size distribution of defect clusters with MD simulations of 150 keV collision cascades in W [6].

All of the above MD simulations of primary damage were performed in single crystal W. To investigate the effect of GBs on primary damage in bcc W, an MD simulation was made in single- and nano-(poly) crystalline W [28]. The simulation results showed that the number of interstitials in the steady state is twice as large in

* Corresponding author at: Key Laboratory for Materials Physics, Institute of Solid State Physics, Chinese Academy of Sciences, Hefei 230031, China.
E-mail address: zzeng@theory.issp.ac.cn (Z. Zeng).

http://dx.doi.org/10.1016/j.jnucmat.2014.11.135
0022-3115/

the nano-crystal, which is in contrast with the fact that GB plays the role of absorbing interstitials; hence, it requires further understanding. In addition, it is not yet clear how the number of defects generated in the primary damage stage changes quantitatively with the PKA distance from the GB plane. Furthermore, as far as we know, there is no detailed information about distributions of defect clusters in the adjacent region of the GB in bcc W. Because such information is very useful for investigating the long-term defect structure evolution and migrating processes, it is necessary to have a detailed study on the effects of GBs in the primary damage stage. The goal of this study is to understand the role of GBs on the defect production and cluster distribution as well as to obtain the differences between single crystal and bi-crystal materials on primary damage. Our results highlight the role played by GB types and temperature in the primary damage stage.

2. Methods

2.1. Theoretical models

We have created five bi-crystal structures in this work. For comparison, two single crystal structures with different volumes have also been constructed. The five bi-crystal GBs include three tilt GBs of $\Sigma5(031)-[100], \Sigma21(1\bar{4}2)-[211], \Sigma85(092)-[100]$ and two twist GBs of $\Sigma5[001]$*Twist* and $\Sigma85[001]$*Twist* [29], which are denoted as $\Sigma5$*Tilt*, $\Sigma21$*Tilt*, $\Sigma85$*Tilt*, $\Sigma5$*Twist*, $\Sigma85$*Twist*, respectively. To release stress in the GB structures, the minimum energy configurations of five GB structures are obtained by applying the conjugate gradient (CG) minimization method under zero external pressure [30], as shown in Fig. 1. Periodic boundary conditions are applied in all three Cartesian directions so that there are two equivalent GBs in the systems, one at the center ($z=0$) and the other at the edge of the simulation box. Atoms close to the GB have visibly different potential energies from the atoms in the bulk region. The width of the GB is thus defined as the region near the dividing interface, which includes atoms with potential energies outside the interval $(1\pm0.003)\cdot E_{coh}$ [31], where E_{coh} of -8.90 eV is the cohesive energy of a W atom according to the potential used. The GB energy can also be calculated according to the expression presented by Pérrez-Pérrez [31]. The basic information on the two single crystal structures and the five GB structures are summarized in Tables 1 and 2, respectively.

2.2. Details of MD simulations

All MD simulations are performed with LAMMPS [32]. The Finnis–Sinclair [33] type Derlet–Nguyen–Manh–Dudarev (DNMD) W potential [34] modified about the repulsive part with ZBL potential [35] at short-range and the electron density function [36] are implemented for this study. The modified potential not only reproduces correct point defect structures and experimentally obtained defect threshold energies but is also suitable for high-energy simulations [36]. Cascades are initiated near the central GB so that the other GB does not interact with the cascades. The MD simulations include two stages. In stage I, the simulation system is relaxed within the NVT ensemble (constant number of atoms, volume, and temperature) for 10 ps with a time step of 1 fs. The thermostat is applied to all atoms in the system at desired temperatures. In stage II, NVE ensemble (constant number of atoms, volume, and total energy) is employed to relax the system for 80 ps. At the beginning of this stage, a kinetic energy of 10 keV or 20 keV is set to a PKA at a certain distance from the central GB plane. During this stage, only the atoms within a shell of approximately 0.3 nm from the outer margin of the simulation box are under the thermostat by applying the velocity rescaling method at the desired temperature. For all of the above MD calculations, energy minimization structures are used as initial configurations. The time step varies from 1×10^{-6} ps to 2×10^{-3} ps depending on the atomic velocities and force magnitude. In all simulations of GB structures, the PKA velocities are along the *z*-axis. For exploring the effects of the initial PKA positions on defect productions, 9 different PKA distances from the GB plane are chosen, ranging from -1.0 nm to 7.0 nm with the same interval of 1.0 nm. Here, a negative distance means that the PKA is on the other side of the GB plane. All simulations, for single crystal and all types of GBs and distances, are performed at 300 K. In addition, simulations at 4.2 K and 900 K in the $\Sigma5$*Tilt* structure and in the single crystal are also conducted to investigate temperature effects on defect production. To reduce the statistical

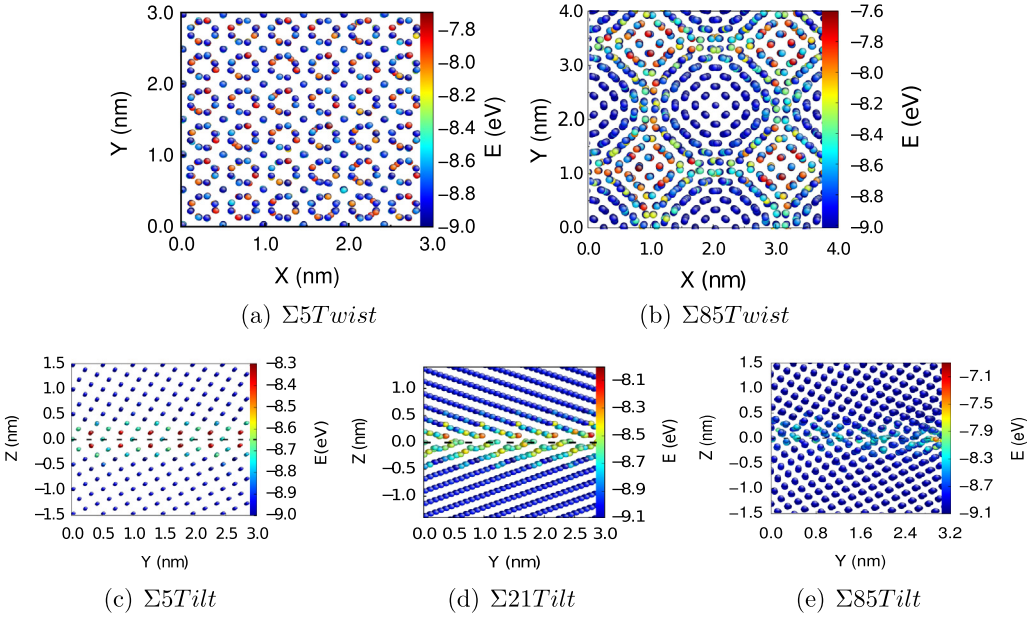

(a) $\Sigma5Twist$ (b) $\Sigma85Twist$ (c) $\Sigma5Tilt$ (d) $\Sigma21Tilt$ (e) $\Sigma85Tilt$

Fig. 1. The stable structure of the five GB types in bcc W selected in this work. The *z*-axis is normal to the GB plane. The two twist GB structures are projected from the *z*-axis, while the three tilt GB structures are projected from the *x*-axis. The visual tool AtomEye [49] was used as the atomistic configuration viewer. Here, atoms are colored with their potential energies, and the corresponding values are shown in the color bar. (For interpretation of the references to color in this figure legend, the reader is referred to the web version of this article.)

Table 1
The single crystal models used in this paper. The volume of the simulation box (V), the number of atoms (N) and cascade energy (E) are listed.

Single crystal	V (nm^3)	N	E (keV)
1	18.991×18.991×18.991	432,000	10, 20
2	31.652×31.652×31.652	2,000,000	50

Table 2
The five GB models used in this paper. The misorientation angle (ϕ), the GB energy (E_{GB}), the GB width (W), the volume of the simulation box (V) and the number of atoms (N) are listed.

Type	ϕ (Degrees)	E_{GB} (J/m^2)	W (nm)	V (nm^3)	N
Σ5*Tilt*	53.1	2.051	0.7	15.839×19.993×20.051	400,000
Σ21*Tilt*	44.4	2.531	0.6	18.927×17.820×20.234	429,824
Σ85*Tilt*	64.9	2.628	0.8	17.497×15.190×23.358	391,680
Σ5*Twist*	36.8	3.301	0.7	16.006×16.007×20.311	327,680
Σ85*Twist*	8.80	2.564	0.6	8.249×8.250×20.283	87,040

error, 10 independent cascade simulations are performed at each PKA distance.

2.3. Defect characteristics

The Wigner–Seitz cells method is used for the identification of point defects. The reference structure is obtained by applying the CG minimization method under zero external pressure. If a cell contains no atom, it indicates a vacancy. If a cell contains more than one atom, then the one that is closest to the reference atom is the center atom and the others are treated as interstitial(s). If the distance from a defect to the GB plane is less than the GB width, then the defect is regarded as belonging to the GB region. Otherwise, the defect is in the bulk region. To characterize defect clusters, two defects are considered as belonging to the same cluster if their separation is less than a given cutoff [37]. The criterion for the identification of vacancy cluster is used according to vacancy–vacancy interaction, which is attractive for the first nearest neighbor (1-nn) and the second nearest neighbor (2-nn) and becomes repulsive or negligible at larger distances. Thus, the cutoff is selected of 2-nn for vacancy clusters and 1-nn for interstitial clusters. It is noted that for this specific range, the modified DNMD W potential used in our study cannot reproduce the instability of di-vacancy in W at 0 K obtained by density functional theory (DFT) calculations due to the shortcomings of empirical potentials, which are representative of a featureless electronic density of states [38]. However, the authors of Ref. [38] have also indicated that the electronic free energy implies that di-vacancy becomes attractive at 1-nn and less repulsive at 2-nn due to the electronic entropy. Moreover, the binding property of di-vacancy has a significant impact on the long-time evolution (∼s) of defects but not on the short-time defect production and evolution (∼ps) at high energy conditions. Therefore, the defect productions calculated from the potential used in this study are credible here. Additionally, our investigation on the influence of the cutoff of vacancy clusters reveals that the size distribution of vacancy clusters shifts slightly to smaller sizes for 1-nn compared to the case of 2-nn. Obviously, this slight shifting has no influence on the qualitative results presented in the following section.

3. Results and discussion

3.1. The time dependence of the number of defects

As shown in Fig. 2, when a W atom is knocked, the number of defects increases rapidly (collision phase) at the beginning and reaches a maximum value (thermal spike phase) at approximately 1.0 ps. Ultimately, most of the displaced atoms recombine with the vacant sites (annealing phase) or are trapped by GB, leaving very few of them as stable defects in the bulk region at approximately 10 ps. The maximum number of interstitials produced in GB structures is greater than that in single crystal structures due to the relatively smaller threshold energy in the GB region. After the annealing phase, the number of vacancies in the bulk region is more than that of interstitials. Fig. 3 shows four snapshots of the collision phase (a), the thermal spike phase (b) and the annealing phase (c and d) corresponding to the process presented in Fig. 2. After 10 ps of annealing, the number of defects reaches a steady value (Fig. 3(c)) with only 2 interstitials and 38 vacancies left in the bulk region at 80.69 ps (Fig. 3(d)). The bulk region is vacancy-rich compared to the interstitial-rich GB region [12,19,39–41]. This bias-absorption for interstitials by GB is due to the difference between the migration energy barriers of interstitials and vacancies in the bulk region. Vacancies may be regarded as immobile in the time scale of ps, whereas interstitials can migrate a large distance through replacement collision sequences (RCS). When interstitials move to the region near the GB, they can be absorbed by it due to the pressure gradient [41–43].

3.2. Defects in the bulk region

The RCS images are shown in Fig. 4, where three representative PKA distances are chosen in the GB Σ21*Tilt* structure and compared to those in the single crystal structure. The thermal spike region is visualized by showing the displacement vectors between atomic positions at 0 ps and 80 ps. There are several long lines in each figure, and each long line is made of serials of displacement vectors head by tail. The head of each long line is an interstitial atom, while the tail is a vacancy. As observed from Fig. 4, the GB has a significant effect on the morphology of the cascades due to the stress gradient [42]. The number of defects produced in the bulk region for different PKA distances from the GB plane is shown in Fig. 5. The defect production is more sensitive to the initial PKA position than to the difference among different GB structures. When the PKA is too far away from the GB to modify defect production (see PKA distance at 7.0 nm in Fig. 5), the numbers of interstitials and vacancies are equal within the standard errors. Such defect production is similar to that in the single crystal structures. The slight offset should be caused by the differences in PKA velocity directions [44]. Equal "red" and "blue" symbols in Fig. 4(c) represent this

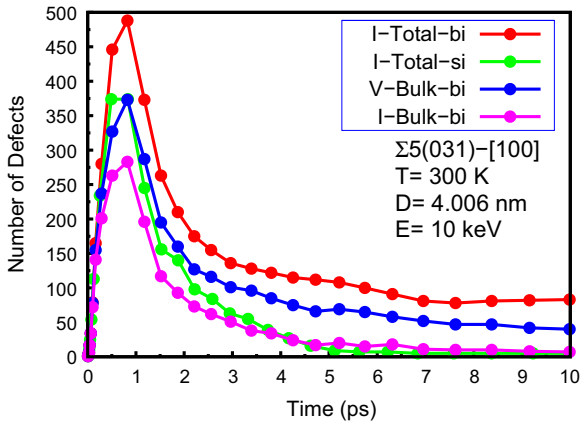

Fig. 2. The time evolution of the number of total interstitials produced in the single crystal (I-Total-si) and GB Σ5*Tilt* structure (I-Total-bi), together with interstitials (I-Bulk-bi) and vacancies (V-Bulk-bi) in the bulk region of the GB Σ5*Tilt* structure. The PKA distance from the GB plane is 4.006 nm. All simulations are conducted at 300 K with a cascade energy of 10 keV.

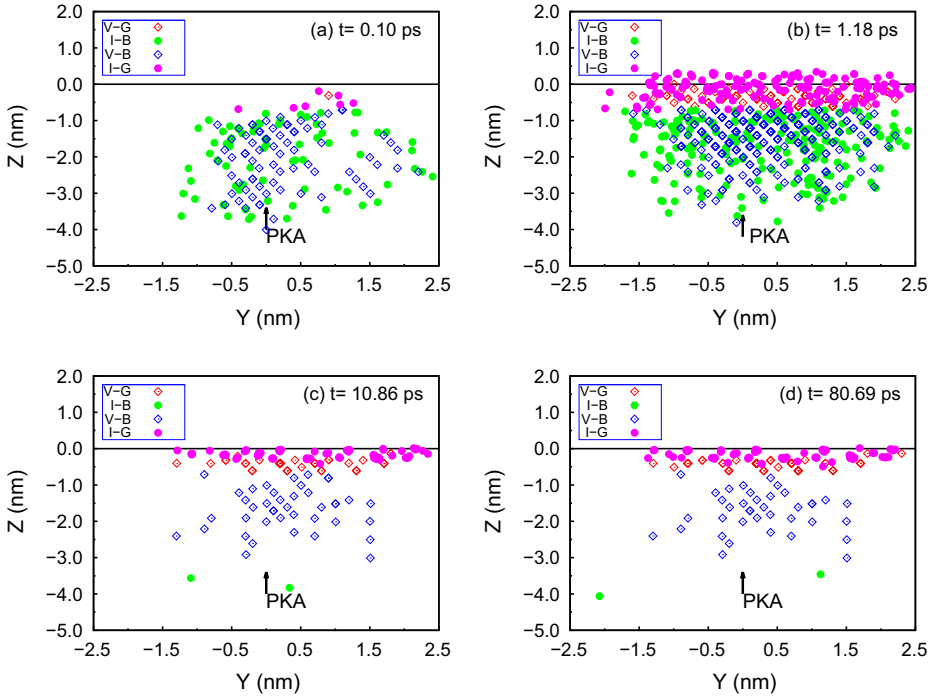

Fig. 3. Four snapshots of the cascade corresponding to Fig. 2. The black line indicates the GB plane. V–G, I–B, V–B and I–G denote vacancy in the GB region, interstitial atom in the bulk region, vacancy in the bulk region and interstitial atom in the GB region, respectively.

case, and its RCS image is very similar to that of the single crystal structure in Fig. 4(d). In other words, without the influence of the GB, interstitials remain in the peripheral region of cascades, whereas vacancies remain in the central region. When the PKA is closer to the GB, the number of vacancies is greater than that of interstitials. Furthermore, the number of vacancies has a maximum peak value when the PKA is approximately 4.0 nm away from the GB. This is the critical distance d_c where the center of the cascade region is far away from the GB, but interstitials can also be absorbed by the GB efficiently, as indicated by many lines directly

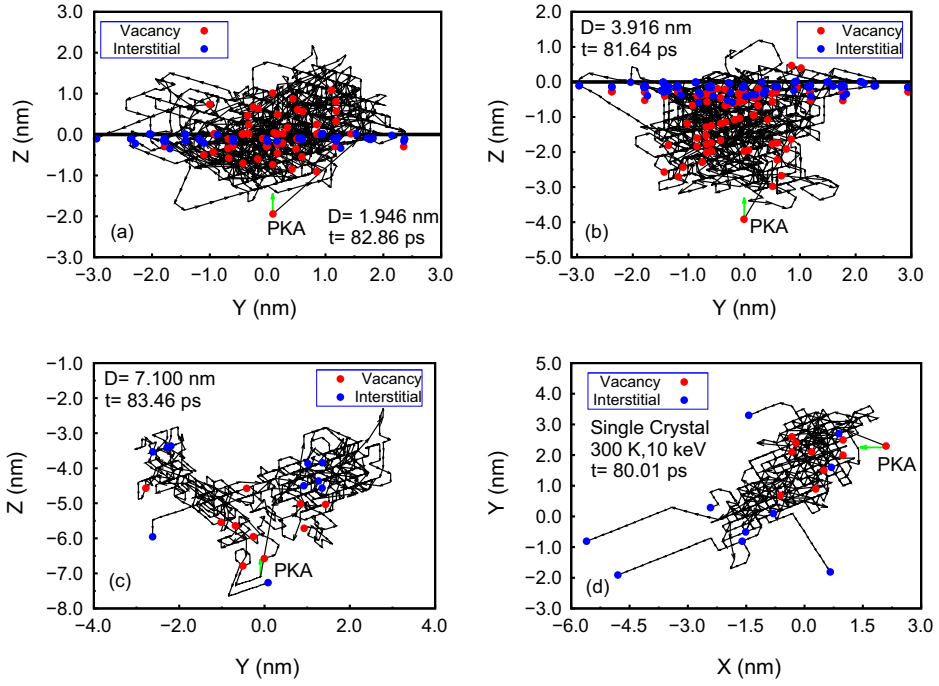

Fig. 4. (a–c) The projection view of the cascade region along the negative *x*-axis showing the GB plane and the displacement vectors generated with cascade energy of 10 keV at 300 K in the GB Σ21*Tilt* structure, with different PKA distances from the GB plane, 1.946 nm (a), 3.916 nm (b) and 7.10 nm (c); (d) The projection view of the cascade region along the negative *z*-axis in the single crystal structure. The red points and blue points represent vacancies and interstitials, respectively. The GB is shown with a thick black line, and the position together with the direction of the PKA is indicated by a green arrow. (For interpretation of the references to color in this figure legend, the reader is referred to the web version of this article.)

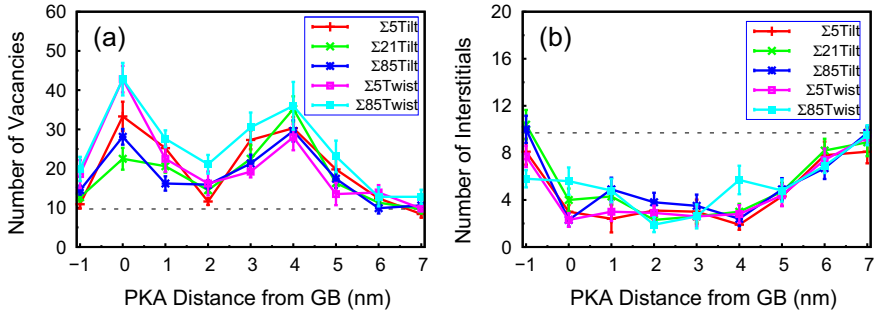

Fig. 5. The variation of the number of defects formed in the bulk region at different PKA distances with cascade energy of 10 keV at 300 K after 80 ps annealing time. (a) Vacancies; (b) interstitials. Each datum point is averaged over 10 independent MD simulations with the error bar representing the standard error. The number of defects obtained from a single crystal structure with the same cascade energy is indicated by the horizontal dashed line.

pointing to the GB in Fig. 4(b). The interstitials are trapped by the GB and thus cannot recombine with unmoved vacancies in the bulk region, which results in a relatively higher number of vacancies. As the PKA gradually approaches the GB, more defects are produced directly within the GB region. At approximately 2.0 nm, the bias-absorption of defects by the GB is not so pronounced and the number of vacancies has a minimum peak value. This distance corresponds to the case where the center of cascade morphology is in the GB region and most displacement vectors overlap with the GB, as shown in Fig. 4(a). In the region close to the GBs, migration barriers of defects are usually reduced compared to those in the bulk region [45,12]. This causes the total absorption of point defects, whereas the interstitials can be absorbed by the GB faster than the vacancies. Only fewer defects are produced in the bulk region when the cascade overlaps maximally with the GB region, which is similar to what was obtained in previous work on Cu [12] and TiO_2 [39]. We could understand the result presented by Ref. [28], which claimed that the number of interstitials is twice as large in nano-crystal W compared to the case in single crystal W. In addition to the reason provided by the authors of that study that this is caused by the attractive interaction between the GB and the interstitials, we could understand it from the following aspects. First, the cascade energy of up to 100 keV used in their work could create more defects, which results in more time lost as the GB absorbs interstitials and may exceed the simulation time. Second, only one simulation result in Ref. [28] might be an accident. Our statistical average among several simulations will have certainly provided stronger evidence. Finally, PKA positions and velocity directions also have an impact on their result.

3.3. Interstitial and vacancy clustering

The cascade energy dependences of in-cascade interstitial and vacancy clustering in single crystal structures at 4.2 K, 300 K and 900 K are shown in Fig. 6. First, the size distribution of interstitial clusters shifts to larger sizes as either the cascade energy or the temperature increases (Fig. 6(a,c,e)). This result is the same as in previous work [46–48]. Second, the size of vacancy clusters increases as the energy of PKA (Fig. 6 (b,d,f)) increases, whereas the dependence on temperature (Fig. 6(b,d,f)) is not obvious. On the one hand, the volume of the cascade increases as the energy of PKA increases, producing more defects. Therefore, for the cascade of PKAs with larger energy, more vacancies remaining in the central region can collapse into larger vacancy clusters. On the other hand, the interstitials can move much longer distances compared to the recorded unmoved vacancies. Therefore, the interstitials are more likely to meet each other and merge into clusters at an elevated temperature, whereas the vacancies still remain unmoved even at higher temperatures, which results in vacancy clustering that is insensitive to the temperature at the primary damage stage.

To understand the important effects of GBs on the interstitial and vacancy clustering, we select two representative PKA distances (2.0 nm and 4.0 nm) corresponding to the minimum and maximum number of vacancies remaining in the bulk region of four GB structures, respectively. As shown in Fig. 7(a) and (c), the total fractions of clusters of different size are not equal to 1.0, which means that no interstitial remains in the bulk region in certain cascade simulations. Furthermore, the interstitial cluster size distribution shifts to smaller sizes compared to the case of the single crystal structure in Fig. 6(a). The behavior of vacancy clustering is quite different from that of interstitial clustering according to Fig. 7(b) and (d). When the cascades are initiated at approximately 2.0 nm away from the GB plane, the distribution of vacancy population in clusters is similar to that of single crystal simulations. Vacancy clusters of size greater than 5 cannot form in any simulation, and the fraction decreases rapidly as the cluster size increases. However, for the cascade at approximately 4.0 nm, the size distribution of vacancy clusters shifts to significantly larger sizes, which is consistent with other MD simulation results [19,43]. When the interaction between the GB and the cascades reaches its maximum extent, which corresponds to the case where the PKA distance is 2.0 nm, the point defects are absorbed by the GB efficiently. Therefore, there is no large interstitial or vacancy cluster formed in the bulk region. In contrast, Fig. 7(d) shows that the GB interacts with a small part of the cascade. On the one hand, at the thermal spike phase, interstitials move toward the GBs via RCS and are absorbed efficiently by the GB [19,43,42]. Therefore, the probability of forming larger interstitial clusters is reduced significantly. On the other hand, the interstitials are trapped by the GBs and thus cannot recombine with the vacancies remaining in the bulk region. Consequently, the more vacancies remaining in the bulk region, the larger are the clusters that can be formed.

We have therefore obtained two characteristics of defect clustering near the GB: (1) the interstitial cluster size distribution shifts to smaller sizes due to the efficient absorption of the interstitials by the GB; and (2) the size distribution of vacancy clusters shifts to larger sizes when the GB interacts with a small part of the cascades.

3.4. The influence of GB type and temperature

As observed in Fig. 5(a), there are significant differences in the number of vacancies produced depending not only on the position of the PKA in the GB region but also on the GB structures. In particular, the two twist GB structures lead to a relatively higher number of vacancies. The interaction between defects and GB is much stronger in the GB region. Therefore, slight differences in proper-

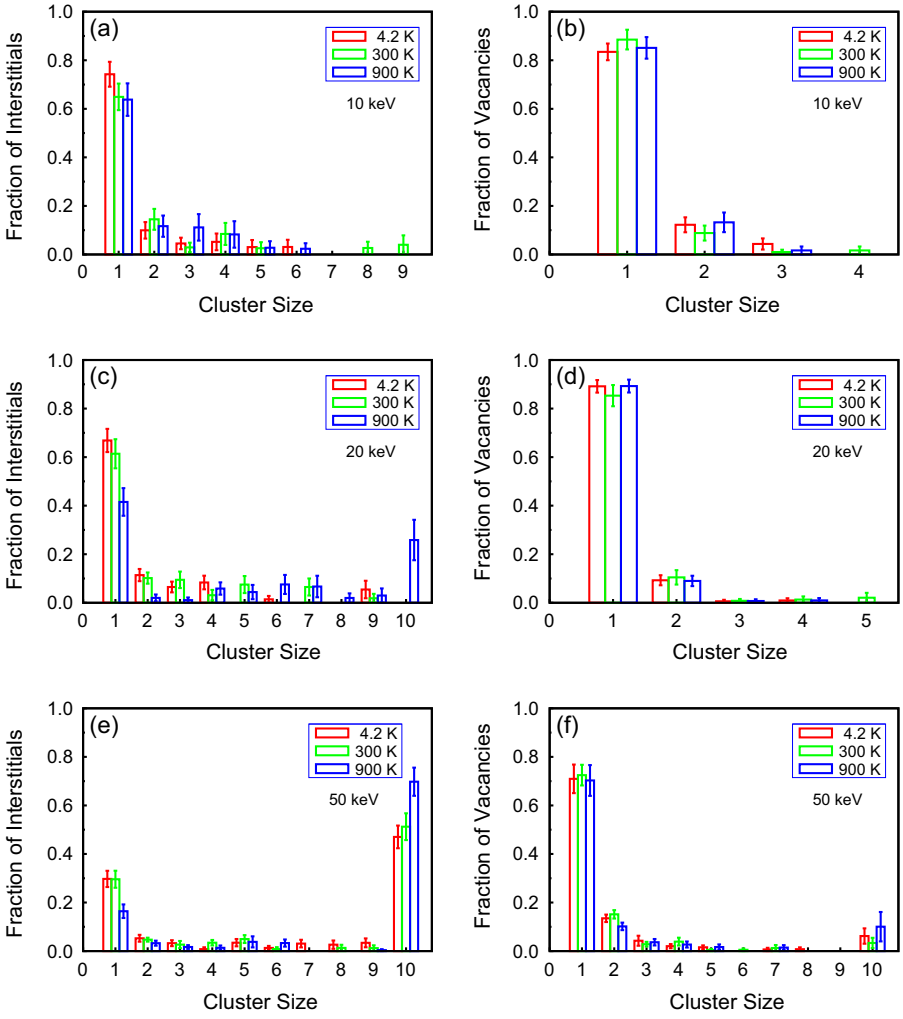

Fig. 6. Fractional size distribution of defect clusters formed in single crystal W with cascade energy of 10 keV (a and b), 20 keV (c and d) or 50 keV (e and f) at different temperatures after 80 ps. The number of defects (interstitials or vacancies) of a particular size is divided by the total number of surviving defects.

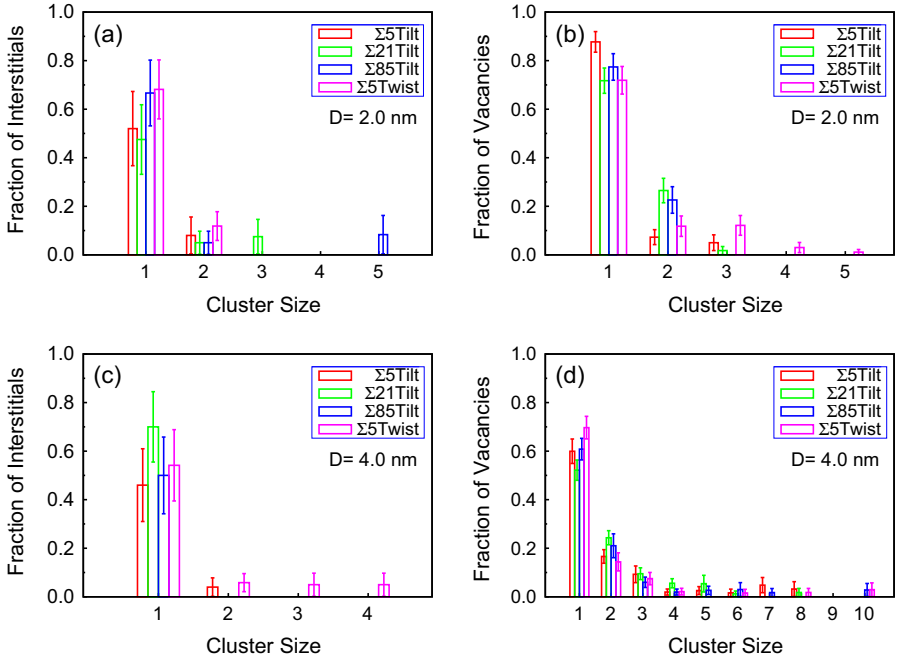

Fig. 7. Fractional size distribution of defect clusters formed in the bulk region of four GB types with cascade energy of 10 keV and PKA distances of 2.0 nm (a and b) or 4.0 nm (c and d) at 300 K after 80 ps.

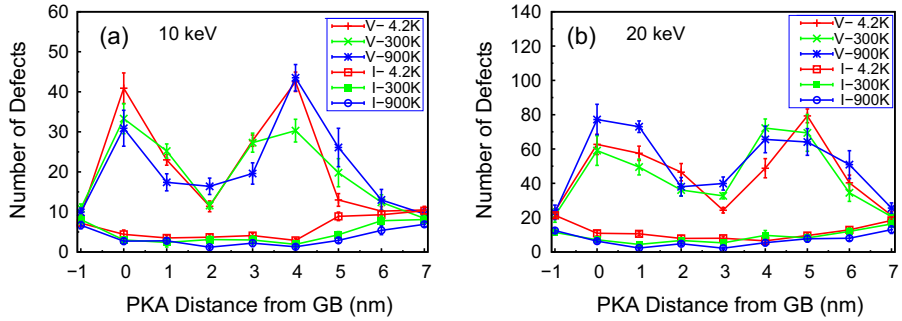

Fig. 8. The variation of the number of defects formed in the bulk region at different PKA distances with cascade energy of 10 keV (a) or 20 keV (b) at different temperatures with regard to the GB Σ5*Tilt* structure after 80 ps of annealing time. Each datum point is averaged over 10 independent MD simulations with the error bar representing the standard error.

ties such as the threshold energy, the defect formation energy and the segregation energy may induce obvious offsets in defect production. Although there are large differences in the number of defects created in the bulk region at some PKA distances, their tendency to change with PKA distance is consistent through all types of GB. Thus, the differences among GB types should be due to the detailed interactions between defects and GB, depending on the GB atomic structure and the stress field near GB.

Fig. 8 illustrates the influence of temperature on the defect production when the GB exists. The trends are not univocal. The number of vacancies increases with increasing temperature at the specific PKA distances of 5.0 nm in Fig. 8 and 3.0 nm in Fig. 8(b), whereas the temperature effect is opposite at other distances, e.g., 1.0 nm in Fig. 8 and 5.0 nm in Fig. 8(b). It is different from the cases obtained from a singe crystal [26,47], where a slight decrease in the Frenkel-pairs number with the increase in temperature is invariably observed. Although it is not straightforward to find an obvious relationship between the number of vacancies and temperature at different PKA distances, it is still apparent that the number of interstitials in the bulk region decreases slightly as temperature increases. On the one hand, the rate at which interstitials recombine with vacancies is enhanced at elevated temperatures. On the other hand, it is easier for interstitials to migrate towards GB at higher temperature. These two effects result in a completely different relationship between the defect production of vacancies or interstitials and temperature when the GB exists. In summary, the number of interstitials decreases with increasing temperature, whereas the qualitative relationship between the number of vacancies created in the bulk region and the temperature is unclear.

4. Conclusion

In this paper, the effects of GB on the primary radiation damage in tungsten are analyzed by performing MD simulations of cascades. It is shown that defect production is sensitive to the specific PKA distance away from GB. On the one hand, there is a bias-absorption of interstitials by GB compared to vacancies, which results in the interstitial cluster size distribution shifting to smaller sizes. On the other hand, the vacancy cluster size distribution shifts to larger sizes, when there is only a limited overlap between the cascade and the GB. There are significant differences in the number of vacancies produced with the location of PKA in the GB region in which two twist GB structures have relatively higher numbers of vacancies. The number of interstitials decreases with increasing temperature. It is expected that the proximity of the GB will affect the rate at which the irradiation-induced defects segregate and annihilate at the GB, a process that would take place on a longer timescale. Long-term damage evolution needs to be considered in future work to determine whether an increased concentration of defects compared to that of a single crystal can be absorbed and annihilated efficiently by nearby GBs.

Acknowledgments

This work was supported by the National Science Foundation of China under Grant Nos. 11275229, 11475215 & NSAF U1230202, the Special Funds for Major State Basic Research Project of China (973) under Grant No. 2012CB933702, the Hefei Center for Physical Science and Technology under Grant No. 2012FXZY004, and Director Grants of CASHIPS. Part of the calculations were performed at the Center for Computational Science of CASHIPS, the ScGrid of Supercomputing Center, and the Computer Network Information Center of the Chinese Academy of Sciences.

References

[1] R.E. Stoller, G.R. Odette, B.D. Wirth, J. Nucl. Mater. 251 (1997) 49.
[2] R.E. Stoller, L.R. Greenwood, J. Nucl. Mater. 271 (1999) 57.
[3] W. Jäger, M. Wilkens, Phys. Stat. Sol. (a) 32 (1975) 89.
[4] M.R. Gilbert, S.L. Dudarev, P.M. Derlet, et al., J. Phys.: Condens. Matter 20 (2008) 345214.
[5] X. Yi, M.L. Jenkins, M. Briceno, et al., Philos. Mag. 93 (2013) 1715.
[6] A.E. Sand, S.L. Dudarev, K. Nordlund, EPL 103 (2013) 46003.
[7] L.K. Mansur, J. Nucl. Mater. 216 (1994) 97.
[8] M. Victoria, N. Baluc, C. Bailat, et al., J. Nucl. Mater. 276 (2000) 114.
[9] K.E. Sickafus, R.W. Grimes, J.A. Valdez, et al., Nat. Mater. 6 (2007) 217.
[10] K.E. Sickafus, L. Minervini, R.W. Grimes, J.A. Valdez, M. Ishimaru, F. Li, K.J. McClellan, T. Hartmann, Science 289 (2000) 748.
[11] G.R. Odette, M.J. Alinger, B.D. Wirth, Annu. Rev. Mater. Res. 38 (2008) 471.
[12] X.M. Bai, A.F. Voter, R.G. Hoagland, M. Nastasi, B.P. Uberuaga, Science 327 (2010) 1631.
[13] Y. Chimi, A. Iwase, N. Ishikawa, M. Kobiyama, T. Inami, S. Okuda, J. Nucl. Mater. 297 (2001) 355.
[14] M. Rose, A.G. Balogh, H. Hahn, Nucl. Inst. Meth. Phys. Res. B 127C128 (1997) 119.
[15] T.D. Shen, S. Feng, M. Tang, J.A. Valdez, Y. Wang, K.E. Sickafus, Appl. Phys. Lett. 90 (2007) 263115.
[16] A. Alsabbagh, R.Z. Valiev, K.L. Murty, J. Nucl. Mater. 443 (2013) 302.
[17] A. Misra, M.J. Demkowicz, X. Zhang, R.G. Hoagland, J. Miner. Met. Mater. Soc. 59 (2007) 62.
[18] M.J. Demkowicz, R.G. Hoagland, J.P. Hirth, Phys. Rev. Lett. 100 (2008) 136102.
[19] M. Samaras, P.M. Derlet, H.V. Swygenhoven, M. Victoria, Phys. Rev. Lett. 88 (2002) 125505.
[20] N.P. Taylora, R. Pampinb, Fusion Eng. Des. 81 (2006) 1333.
[21] M. Rieth, J.L. Boutard, S.L. Dudarev, et al., J. Nucl. Mater. 417 (2011) 463.
[22] H. Bolt, V. Barabash, W. Krauss, et al., J. Nucl. Mater. 329-333 (2004) 66.
[23] S. Zinkle, M. Victoria, K. Abe, J. Nucl. Mater. 307-311 (2002) 31.
[24] S. Fukuzumi, T. Yoshiie, Y. Satoh, Q. Xu, H. Mori, M. Kawai, J. Nucl. Mater. 343 (2005) 308.
[25] H.W. Wang, Y. Gao, E.G. Fu, et al., J. Nucl. Mater. 442 (2013) 189.
[26] J. Fikar, R. Schäublin, Nucl. Inst. Meth. Phys. Res. B 255 (2007) 27.
[27] T. Troev, N. Nankov, T. Yoshiie, Nucl. Inst. Meth. Phys. Res. B 269 (2011) 566.
[28] N.-Y. Park, P.-R. Cha, Y.-C. Kim, et al., Met. Mater. Int. 15 (2009) 447.
[29] H. Ogawa, Mater. Trans. 47 (2006) 2706.
[30] M. Parrinello, A. Rahman, J. Appl. Phys. 52 (1981) 7182.
[31] F.J. Pérrez-Pérrez, R. Smith, Nucl. Inst. Meth. Phys. Res. B 164-165 (2000) 487.
[32] S. Plimpton, J. Comput. Phys. 117 (1995) 1.

[33] M.W. Finnis, J.E. Sinclair, Phil. Mag. A 50 (1984) 45.
[34] P.M. Derlet, D. Nguyen-Manh, S.L. Dudarev, Phys. Rev. B 76 (2007) 054107.
[35] J.F. Ziegler, J.P. Biersack, U. Littmark, The Stopping and Range of Ions in Matter, Pergamon, New York, 1985.
[36] C. Björkas, K. Nordlund, S. Dudarev, Nucl. Inst. Meth. Phys. Res. B 268 (2010) 1529.
[37] S. Stoddard, J. Comput. Phys. 27 (1978) 291.
[38] L. Ventelon, F. Willaime, C.C. Fu, et al., J. Nucl. Mater. 425 (2012) 16.
[39] X.M. Bai, B.P. Uberuaga, Phil. Mag. 92 (2012) 1469.
[40] X.M. Bai, L.J. Vernon, R.G. Hoagland, A.F. Voter, M. Nastasi, B.P. Uberuaga, Phys. Rev. B 85 (2012) 214103.
[41] K. Sugio, Y. Shimomura, T.D. de la Rubia, J. Phys. Soc. Jpn. 67 (1998) 882.
[42] M. Samaras, P.M. Derlet, H.V. Swygenhoven, M. Victoria, Phys. Rev. B 68 (2003) 224111.
[43] M. Samaras, P.M. Derlet, H.V. Swygenhoven, M. Victoria, Phil. Mag. 83 (2003) 3599.
[44] Q. Xu, T. Yoshiie, H.C. Huang, Nucl. Inst. Meth. Phys. Res. B 206 (2003) 123.
[45] X.Y. Li, W. Liu, C.S. Liu, et al., Nucl. Fusion 53 (2013) 123014.
[46] C. Björkas, K. Nordlund, S. Dudarev, Nucl. Inst. Meth. Phys. Res. B 267 (2009) 3204.
[47] D.J. Bacon, F. Gao, Y.N. Osetsky, Nucl. Inst. Meth. Phys. Res. B 153 (1999) 87.
[48] R.E. Stoller, J. Nucl. Mater. 276 (2000) 22.
[49] J. Li, Modell. Simul. Mater. Sci. Eng. 11 (2003) 173.